NeuroImage 43 (2008) 528–539

Contents lists available at ScienceDirect

NeuroImage

journal homepage: www.elsevier.com/locate/ynimg

Small-world and scale-free organization of voxel-based resting-state functional connectivity in the human brain

M.P. van den Heuvel [a,*], C.J. Stam [b], M. Boersma [b], H.E. Hulshoff Pol [a]

[a] Rudolf Magnus Institute of Neuroscience, University Medical Center Utrecht, Department of psychiatry, Utrecht, The Netherlands
[b] Institute for Clinical and Experimental Neurosciences, Department of Clinical Neurophysiology, VU University Medical Center, Amsterdam, The Netherlands

ARTICLE INFO

Article history:
Received 9 April 2008
Revised 22 July 2008
Accepted 6 August 2008
Available online 22 August 2008

ABSTRACT

The brain is a complex dynamic system of functionally connected regions. Graph theory has been successfully used to describe the organization of such dynamic systems. Recent resting-state fMRI studies have suggested that inter-regional functional connectivity shows a small-world topology, indicating an organization of the brain in highly clustered sub-networks, combined with a high level of global connectivity. In addition, a few studies have investigated a possible scale-free topology of the human brain, but the results of these studies have been inconclusive. These studies have mainly focused on inter-regional connectivity, representing the brain as a network of brain regions, requiring an arbitrary definition of such regions. However, using a voxel-wise approach allows for the model-free examination of both inter-regional as well as intra-regional connectivity and might reveal new information on network organization. Especially, a voxel-based study could give information about a possible scale-free organization of functional connectivity in the human brain. Resting-state 3 Tesla fMRI recordings of 28 healthy subjects were acquired and individual connectivity graphs were formed out of all cortical and sub-cortical voxels with connections reflecting inter-voxel functional connectivity. Graph characteristics from these connectivity networks were computed. The clustering-coefficient of these networks turned out to be much higher than the clustering-coefficient of comparable random graphs, together with a short average path length, indicating a small-world organization. Furthermore, the connectivity distribution of the number of inter-voxel connections followed a power-law scaling with an exponent close to 2, suggesting a scale-free network topology. Our findings suggest a combined small-world and scale-free organization of the functionally connected human brain. The results are interpreted as evidence for a highly efficient organization of the functionally connected brain, in which voxels are mostly connected with their direct neighbors forming clustered sub-networks, which are held together by a small number of highly connected hub-voxels that ensure a high level of overall connectivity.

© 2008 Elsevier Inc. All rights reserved.

Introduction

The brain is a complex dynamic system in which information is continuously processed and transferred to other interconnected regions with correlated functional dynamics (Sporns et al., 2004, 2000). The temporal dependence of neuronal activity between different brain regions is known as functional connectivity (Aertsen et al., 1989; Friston et al., 1993) and is widely investigated by measuring the coherence of resting-state BOLD fMRI time-series. Of special interest are the low frequency oscillations (~0.01–0.1 Hz) of BOLD fMRI time-series recorded during rest, as they have been observed to show correlated patterns between anatomically separated brain regions (Biswal et al., 1995; Cordes et al., 2000; Lowe et al., 2000). There is an ongoing debate on whether these resting-state BOLD signals predominantly result from physiological processes, like respiratory and cardiac oscillations (Birn et al., 2006; Wise et al., 2004) or whether these correlations originate from synchronization in the underlying neuronal activation patterns of these regions observed through a hemodynamic response function (Buckner and Vincent, 2007; Greicius et al., 2003; Gusnard et al., 2001). The latter view is supported by the observation that most of these correlations occur between cortical regions that are known to participate in the same functional network, for example regions of the motor, visual and auditory network (Biswal et al., 1997; Cordes et al., 2000; Fox and Raichle, 2007; Greicius et al., 2003). In addition, within cortical regions, these observed spontaneous BOLD patterns are mainly dominated by lower frequencies (<0.1 Hz), with a minimal contribution of higher cardiac and respiratory oscillations (Cordes et al., 2001, 2000). Furthermore, recently spontaneous BOLD fluctuations have been found to correlate with concurrent fluctuations in neuronal spiking, suggesting a direct link between resting-state time-lag BOLD

* Corresponding author.
E-mail address: M.P.vandenheuvel@umcutrecht.nl (M.P. van den Heuvel).

1053-8119/$ – see front matter © 2008 Elsevier Inc. All rights reserved.
doi:10.1016/j.neuroimage.2008.08.010

signals and intrinsic neuronal activity (Shmuel and Leopold, 2008). In this context, it is believed that the resting-state BOLD fluctuations of cortical and sub-cortical regions, at least in part, originate from intrinsic neuronal activity (Biswal et al., 1995; Greicius et al., in press; Gusnard et al., 2001; Shmuel and Leopold, 2008) and that the observed temporal coherence between anatomically separated regions is reflecting synchronization between the underlying neuronal activation patterns of these regions. Regions that show such a synchronized behavior are suggested to form functional resting-state brain networks (Beckmann et al., 2005; Biswal et al., 1995, 1997; Cordes et al., 2001; Damoiseaux et al., 2006; Fox et al., 2005; Greicius et al., 2003; Gusnard et al., 2001; Horwitz et al., 2005; Kiviniemi et al., 2003; Salvador et al., 2005b; Sun et al., 2004; Thirion et al., 2006; Van den Heuvel et al., 2008; Xiong et al., 1999).

To further probe the complex structure of functional brain networks a well-defined theoretical framework is needed. Biological systems can be represented as complex networks and examined by using 'graph theory'. A graph $G=(V,E)$ is a mathematical description of a network, consisting of a collection of elements (nodes) V and connections (edges) E interconnecting the nodes of the graph. Within this approach, the functionally connected brain can be represented as a network of regions with connections describing inter-regional functional connectivity (Salvador et al., 2005b; Sporns et al., 2000; Stam et al., 2003). Examining the connectivity architecture of the human brain may provide important information about its organization and function (Sporns et al., 2004), as the organization of a network is directly linked to its level of robustness, capability to integrate information and communication efficiency (Buzsaki and Draguhn, 2004; Grigorov, 2005; Latora and Marchiori, 2001; Mathias and Gopal, 2001). Two classes of networks are of special interest. *Small-world* networks are characterized by a high level of clustering and a short average node-to-node distance (Watts and Strogatz, 1998). In addition, *scale-free* networks are characterized by an average low number of connections per node, but with the existence of a small number of highly connected nodes that ensure a high level of global connectivity (Barabasi and Albert, 1999; Barabasi and Bonabeau, 2003). Small-world and scale-free organized networks are known to show a robust network architecture in which information can be transferred and integrated with a high level of efficiency (Latora and Marchiori, 2001; Mathias and Gopal, 2001; Sporns et al., 2004), forming an attractive model for the functionally connected human brain (Achard et al., 2006; Liu et al., 2008; Sporns and Zwi, 2004).

The most important properties that describe the topology of complex networks and characterize whether networks are small-world and/or scale-free organized are the distribution of the number of connections, the level of clustering and the average path length between the nodes of the network (Grigorov, 2005). The connectivity distribution $P(k)$ provides information about the connectivity organization of a network and is defined as the probability that a node is connected to k other nodes in the network. Furthermore, the clustering-coefficient C of a graph describes the connectedness of the direct neighbors of the nodes and gives information on the formation of sub-graphs within the full network. The characteristic path length L is defined as the average shortest path between each two nodes in the graph and gives information on the global level of connectedness of a network. Together, $P(k)$, C and L provide important information about the connectivity topology of a network. *Scale-free* networks are characterized by a connectivity distribution that follows a power-law scaling $P(k) \sim k^{-\gamma}$, indicating that most of the nodes have only a limited number of connections, but that a small number of so-called hub-nodes have a large number of connections and are holding the network together (Barabasi and Albert, 1999; Grigorov, 2005). This in contrast to random connected networks, in which on average all nodes have the same number of connections (Barabasi and Albert, 1999; Grigorov, 2005). Furthermore, random connected networks have a low clustering-coefficient, suggesting a low formation of connected sub-graphs and a short average path length L, indicating that two nodes are never really far apart. *Small-world* organized networks show highly connected sub-networks, resulting in a high clustering-coefficient C, but still with a high level of global connectivity, as indicated by a typical short average path length L (Sporns et al., 2004; Watts and Strogatz, 1998). In general, small-world networks are characterized by a much higher clustering-coefficient than that of random organized networks, but still with an average path length that is of the same length of that of a random network (Watts and Strogatz, 1998). More formally, a small-world network is characterized by a ratio gamma (γ) between the clustering-coefficient Cnet and the clustering-coefficient Crandom of a random graph of >1 and a ratio lambda (λ) between the path length Lnet and the path length Lrandom of a random graph of ≈ 1. The small-world-ness of a graph can be expressed in a single parameter sigma, defined as the ratio between gamma and lambda. Sigma is typically >1 for networks with a small-world organization (Humphries et al., 2006).

A small number of studies have successfully investigated the small-world organization of resting-state functional connectivity using EEG, MEG and resting-state fMRI recordings, in both animal (Sporns and Zwi, 2004) and human studies (Achard and Bullmore, 2007; Achard et al., 2006; Breakspear et al., 2003; Eguiluz et al., 2005; Liu et al., 2008; Micheloyannis et al., 2006; Salvador et al., 2005a; Stam, 2004). Furthermore, functional networks have been suggested to overlap with underlying structural networks (Honey et al., 2007), suggesting that a small-world topology might be a general organization principle of the human brain. However, fMRI imaging studies have been less conclusive about a possible scale-free topology of the human brain. Eguiluz et al. (2005) have reported a scale-free organization of the functionally connected brain on a voxel scale during the performance of a number of simple motor and auditory tasks, but a recent paper of Achard et al. (2006) demonstrated a small-world organization of inter-regional connectivity, but not a scale-free architecture. However, most resting-state fMRI studies have focussed on inter-regional connectivity, examining the functional brain as a network of a fixed number of around 90 regions (Achard and Bullmore, 2007; Achard et al., 2006; Liu et al., 2008; Salvador et al., 2005a), reducing the data from a voxel resolution to a regional resolution. These studies have not taken into account intra-regional connectivity and functional interactions between sub-parts of brain regions. Examining the organization of the functionally connected resting brain on a voxel scale could provide additional information on the characteristics of the functionally connected brain. Especially, a voxel-wise approach could give more insight in a possible scale-free organization of the human brain.

In this study, the organization of the functionally connected human brain during a resting state was examined on a voxel scale. This resulted in a fine-grained representation of the functionally connected human brain in around 10 000 voxels, rather than in the often used template driven parcellated representation of around 90 regions (Achard and Bullmore, 2007; Achard et al., 2006; Liu et al., 2008; Salvador et al., 2005a). Resting-state BOLD fMRI was acquired in 28 healthy subjects on a 3 Tesla MR scanner. For each individual dataset, a functional connectivity graph was formed out of all cortical and sub-cortical voxels, with the pair-wise correlation between the resting-state fMRI time-series as weighted connections between all voxels. From these individual connectivity networks a number of graph characteristics were computed, including the clustering-coefficient C and characteristic path length L and compared to the topology of random graphs with a similar connectivity degree and distribution (Watts and Strogatz, 1998). The small-world index was calculated as a marker of small-world organization (Humphries et al., 2006). Furthermore, the connectivity degree distribution $P(k)$ was examined as an indication of a possible scale-free organization of the functionally connected brain (Barabasi and Albert, 1999; Grigorov, 2005).

Materials and methods

Subjects

Data was acquired on a 3 Tesla Philips Achieva Medical scanner (Philips Medical Systems, Best, The Netherlands) at the University Medical Center Utrecht, The Netherlands. 28 healthy subjects with no psychiatric history (age mean/std: 25.1/7.1; gender: 14 male, 14 female) participated in this study after providing written informed consent as approved by the medial ethics committee for research in humans (METC) of the University Medical Center Utrecht, The Netherlands. During the resting-state fMRI, the scanner room was darkened and subjects were instructed to relax with their eyes closed and think of nothing in particular without falling asleep.

Directly after the resting-state experiment the subjects were asked if they had not fallen asleep during the scanning session. Subjects who reported to have fallen asleep or reported to be close to falling asleep were excluded and a new subject was included as a replacement, resulting in the described group of 28 subjects.

Acquisition

Resting-state blood oxygenation level dependent (BOLD) signals were recorded during a period of 8 min using a fast fMRI sequence (3D PRESTO (Golay et al., 2000; Neggers et al., 2008), acquisition parameters: TR/TE 22 ms/32 ms using shifted echo, flipangle of 9°; SENSE p/s reduction 2/2; a dynamic scantime of 0.5 s, 1000 timeframes, total duration 8 min; FOV 256×256 mm, isotropic voxelsize 4 mm, 32 slices were acquired covering the whole brain). The high temporal acquisition was used to minimize possible back-folding effects (i.e. aliasing) of respiratory and cardiac oscillations (~0.3 Hz and ~0.9–1.0 Hz, respectively) into the lower resting-state frequencies of interest (0.01–0.1 Hz). Directly after the functional time-series an additional PRESTO scan with a better anatomical contrast was acquired (due to an increased flipangle of 25°, FA25) for co-registration purposes. In addition, a T1 weighted image was acquired for anatomical reference (3D FFE, acquisition parameters: TR/TE 10 ms/4.6 ms, SENSE p/s reduction 1.7/1.4; FOV 256×256 mm, voxelsize 0.75×0.75×0.8 mm, 200 slices).

Preprocessing

All fMRI preprocessing steps were done with the SPM2 software package (http://www.fil.ion.ucl.ac.uk). First, the fMRI time-series were realigned to the last functional scan to correct for possible head-motion during the rest experiment. Registration to the last functional scan was used to maximize the spatial overlap of the fMRI time-series with the FA25 scan. The realigned time-series were then coregistered to the FA25 scan, using the last functional scan as a source and the FA25 scan as a target. The T1 image was coregistered to the FA25 scan, to provide spatial alignment between the functional time-series and the anatomical image. Next, the T1 image and the fMRI time-series were normalized to standard space, using the MNI 305 T1 brain (Collins et al., 1994) as a template and the T1 image as a source. The T1 and fMRI time-series were normalized to correct for anatomical variation between the subjects, as possible differences in anatomical structure (e.g. the total number of (sub)-cortical voxels) could affect the graph analysis. It should be noted that the spatial normalization of fMRI time-series involves the interpolation of fMRI voxels and this could introduce (local) artificial correlations between voxels that are related to spatial smoothing and not to functional connectivity. To minimize further interpolation, no spatial filtering was applied to the fMRI time-series.

After registration, the functional time-series were bandpass filtered with a finite impulse response (FIR) bandpass filter to select the low resting-state frequencies of interest (0.01–0.1 Hz). The relatively high sampling-rate of the used resting-state fMRI PRESTO sequence enabled the proper sampling of cardiac and respiratory signals. Band-pass filtering minimized the influence of low frequency MR scanner noise (e.g. slow scanner drifts, typical <0.01 Hz) and high frequency oscillations of cardiac or respiratory signals up to 1 Hz (0.1–1 Hz) (Cordes et al., 2001). Due to the nature of the PRESTO signal, PRESTO fMRI images have a low anatomical contrast between white matter and grey matter (Neggers et al., 2008; Ramsey et al., 1998). Therefore, cortical and sub-cortical voxels were selected based on a cortical segmentation of the T1 image. Cortical segmentation of the T1 was performed with the widely used and freely available Freesurfer software package (http://surfer.nmr.mgh.harvard.edu/). The segmentation maps were resliced to the 4×4×4 mm resolution of the resting-state fMRI times-series. For each individual dataset, the cortical segmentation was visually checked by overlapping the individual cortical segmentation map on the individual T1 image to verify a proper grey matter classification. No large misclassification of white matter or cerebral spinal fluid (CSF) voxels as grey matter voxels was found in any of the individual T1 images. Supplementary Fig. 1 shows the cortical segmentation map of one of the subjects overlaid on the individual T1 image (Supplementary Fig. 1a) and a 4×4×4 resliced version overlapped on one of the PRESTO fMRI images of this subject (Supplementary Fig. 1b). Finally, the resliced segmentation maps were normalized to standard space, using the normalization parameters of the T1 image, to overlap the filtered normalized fMRI time-series.

After preprocessing, the resting-state functional time-series were analyzed using a graph-theoretical approach. For each individual functional dataset, a graph *G*net was constructed out of all cortical and sub-cortical voxels and graph characteristics of *G*net were calculated (see below). In summary, from *G*net the clustering-coefficient *C*net, the characteristic path length *L*net and the distribution degree *P(k)* was calculated. *C*net and *L*net were compared to the clustering-coefficient and path length (i.e. *C*random and *L*random) of a number of random graphs with a number of nodes *k* and a degree distribution *P(k)* similar to that of *G*net. Furthermore, the ratios gamma and lambda were computed as well as the small-world index (Humphries et al., 2006) as an indication of a possible small-world organization. The connectivity distribution of *G*net was computed as the occurrence probability *P(k)* of nodes of degree *k* in *G*net and fitted a power-law function as an indication of a possible scale-free organization of the functionally connected brain at a voxel scale.

Graph analysis

Graph formation

For each individual functional dataset, a connectivity graph *G*net=*(V,E)* was formed, with *V* the collection of *N* grey matter voxels and *E* the collection of connections (edges) between the functionally connected voxels. *N* varied around 10 000 across the groups of subjects. Fig. 1 illustrates the various steps of the applied graph analysis. The first step (Fig. 1, panel a) consisted of the computation of the zero-lag temporal correlations between the filtered resting-state time-series of all voxel-pairs, believed to reflect the level of inter-voxel functional connectivity. These inter-voxel correlations were represented as a correlation matrix *M* with cell *M(i,j)* holding the zero-lag temporal correlation between the fMRI time-series of voxel *i* and voxel *j* (Fig. 1, panel b). Next, *M* was thresholded by a threshold *T*, setting all cells of *M* to 1 that exceeded the threshold and all cells to 0 that did not exceed this threshold, resulting in a binary valued matrix *B* (Fig. 1, panel c). This procedure resulted in the conversion of *M* in an unweighted graph *G*net (Fig. 1, panel d). In this, *G*net=*(V,E)* represented a network of all sub-cortical and cortical voxels of the brain with connections *E* between all functionally connected voxels.

T varied between 0 and 0.7 (with steps of 0.05). With increasing *T* more and more edges were removed from *G*net making the graph

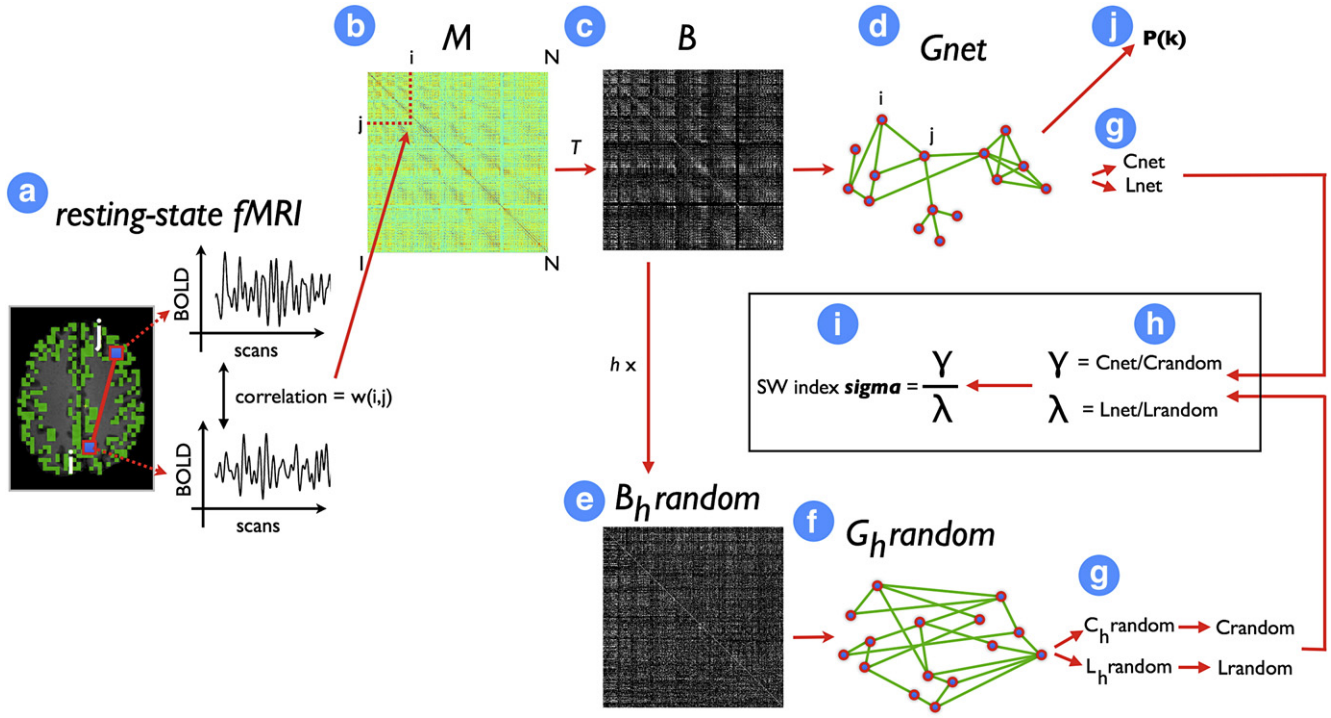

Fig. 1. Schematic illustration of the graph analysis. The first step (panel a) consisted of calculating the temporal zero-lag correlations between the filtered fMRI BOLD time-series of all voxels, which was believed to reflect inter-voxel functional connectivity. The computed correlations were represented as a correlation matrix *M*, with cell *M(i,j)* holding the level of functional connectivity between voxel *i* and voxel *j* (panel b). *M* was thresholded with a threshold *T* (panel c), resulting in a binary connectivity matrix *B*, representing an unweighted graph *G*net (panel d). *T* varied between 0 and 0.7 (with steps of 0.05) and a range of fixed *k* between 4000 and 20. For each fixed *k*, *M* was thresholded with a computed *T* that corresponded exactly to a connectivity degree of *k* for that particular individual dataset. Next, *B* was randomized (panel e) to create a random graph *G*random, with a similar connectivity distribution *P(k)* as *G*net, but with a random organization of connections. *h* random graphs were formed per *G*net. From *G*random and *G*net the graph characteristics *C*net, *L*net, *C*random, *L*random were computed (panel g). *C*random and *L*random were created by averaging the clustering-coefficient and path length of the *h* random graphs. Next, γ and λwere computed, defined as *C*net/*C*random and *L*net/*L*random (panel h), as well as the small-world index sigma as the ratio between γ and λ (SW index, panel i) expressing the small-world-ness of *G*net. In addition, the connectivity distribution *P(k)* of *G*net was computed (panel j). Finally, the individual computed graph characteristics were averaged over the group of subjects and the group averaged connectivity distribution *P(k)* was fitted a power-law function to examine a possible scale-free organization of the functionally connected human brain.

more and more sparse. Increasing *T* would eventually lead to disconnecting voxels from the total graph (i.e. removing all the edges from a voxel). The maximum *T* was empirically set to 0.7 to minimize the number of disconnected voxels to a maximum of 2% of the total amount of voxels in *G*net over the group of subjects. In addition, for each threshold *T*, the size of the largest connected component was computed to verify whether setting threshold *T* would lead to the formation of one large connected component, rather than the formation of multiple relatively large but mutually disconnected components. For all thresholds *T* the largest connected cluster included more than 90% of all nodes in *G*net over the group of subjects, indicating that thresholding with threshold *T* indeed resulted in the formation of one large connected component with only a small number of disconnected voxels for all used thresholds of *T* (data shown in Supplementary Fig. 2a). For each individual dataset, thresholding connectivity matrix *M* with increasing *T* resulted in 15 binary thresholded connectivity matrices (i.e. *B)* representations of *G*net, thresholded with increasing *T*. In addition, to account for possible varying effects of *T* on the individual connectivity graphs, the connectivity matrices were also thresholded as a function of the average connection degree *k* of *G*net. *k* was varied for 15 different settings between 4000 and 20 and for each *k* the *G*net was thresholded with the individual *T* that exactly corresponded to the selected *k*. This resulted in an additional 15 unweighted graphs *G*net for each individual dataset. For $4000 \leq k \leq 50$ the largest connected group of nodes consisted of more than 90% of the total group of nodes (Supplementary Fig. 2b). For the lowest number of $k=20$, the largest connected group of nodes consisted of 83% of all nodes in *G*net (Supplementary Fig. 2b).

Network characteristics

Next, the organizational characteristics of *G*net were calculated, including the *clustering-coefficient C*net, *characteristic path length L*net and the *connectivity distribution P(k)*.

The clustering-coefficient C_i of node *i* expresses the level of connectedness of the direct neighbors of node *i* and gives information on whether they form a connected subgroup in the total network. The clustering-coefficient C_i of voxel *i* is defined as the ratio of the number of edges between the neighbors of voxel *i* and the total number of possible edges between its neighbors. *C*net is defined as the average clustering-coefficient over all voxels in the graph (Sporns et al., 2004; Watts and Strogatz, 1998):

$$Cnet = \frac{1}{N}\sum_{i \in G} C_i \quad (1)$$

with

$$C_i = \frac{\text{edges in } G_i}{\frac{1}{2}k_i(k_i - 1)} \quad (2)$$

and G_i the sub-graph of neighbors of voxel *i* and k_i the number of edges of voxel *i*.

The characteristic path length *L*net of a graph is defined as the averaged minimal distance between each two voxels in the graph and expresses how well the graph is connected globally. Taken distance *d(i,j)* the minimum distance between voxel *i* and *j* as the minimal number of edges that have to be crossed to travel from

voxel i to voxel j, Lnet is defined as the average distance over all voxel-pairs. Formally,

$$L\text{net} = \frac{1}{N(N-1)} \sum_{i \neq j, i,j \in G} d(i,j) \quad (3)$$

for all i and j in Gnet with N the number of voxels in Gnet.

With increasing T more and more paths are removed from Gnet and this could result in disconnecting voxel i from the graph, giving an infinite distance $d(i,j)$ between voxel i and all other voxels in Gnet. Therefore, disconnected voxels could have an effect on the computation of Lnet and Cnet. In this study, this effect was believed to be minimal, as the maximum T was selected to result in a maximum of only ≈200 (2% of the size of Gnet) disconnected voxels. To verify this believed minor effect, two solutions for handling with disconnected voxels were explored for the computation of Lnet. First, all disconnected voxels were removed from the graph, which would probably lead to a small underestimation of Lnet, as the maximum distances $d(i,j)$ are removed. Second, all disconnected voxels were given a distance of the maximum distance in Gnet+1, which would result in a small overestimation of Lnet. As expected, due to the fact that at maximum only 2% of the voxels in Gnet were disconnected, the two different solutions did not change the nature of the Lnet results, indicating that the disconnected voxels had only a minimal effect on the computation of Lnet. For the computation of Cnet two solutions were explored. First, disconnected voxels were removed from the computation of Cnet, which would lead to an overestimation of Cnet as low connected nodes are ignored. Second, the disconnected voxels were given the absolute minimum of clustering-coefficient, i.e. a C_i of 0, which would lead to a small underestimation of Cnet. Similar to the computation of Lnet, these two methods of handling with disconnected voxels did not change the nature of the results of Cnet. This was believed to result from the fact that at maximum only 2% of the voxels in Gnet were disconnected.

Cnet and Lnet express key characteristics of a graph, indicating whether the nodes of the graph are connected in a random or small-world order (Watts and Strogatz, 1998). Random networks are characterized by a low clustering-coefficient Crandom, indicating a limited formation of clustered sub-networks. Random networks have a more global connected character, indicated by a typical short path length Lrandom. In contrast, small-world networks show a high level of local ordering, indicating the formation of sub-graphs, but still with an average short path length of around the same length as the path length of random organized networks, ensuring an optimal level of global connectivity (Latora and Marchiori, 2001). Networks are called small-world if $C\text{net} \gg C\text{random}$ and $L\text{net} \approx L\text{random}$, with Crandom defined as the clustering-coefficient of a random network Grandom of similar size of Gnet (Sporns, 2006; Sporns et al., 2004) and with a similar average connection degree k and connectivity distribution $P(k)$ as Gnet (Sporns and Zwi, 2004; Stam and Reijneveld, 2007). Similar, Lrandom is defined as the characteristic path length of Grandom (Watts and Strogatz, 1998). Small-world networks typically show a ratio gamma (γ) between Cnet and Crandom of >1, and a ratio lambda λ between Lnet and Lrandom of ≈1. γ and λ are formally given by:

$$\gamma = \frac{C_p^{net}}{C_p^{random}} \quad (4)$$

$$\lambda = \frac{L_p^{net}}{L_p^{random}}. \quad (5)$$

The small-world-ness of a graph can be expressed in the small-world index sigma, expressing the level of small-world-ness of a graph as the ratio between γ and λ (Humphries et al., 2006). Sigma is typically >1 for networks with a small-world organization (Humphries et al., 2006).

The connectivity distribution $P(k)$ of Gnet describes the probability that voxel i is connected to k other voxels in the graph and gives insight in the overall connectivity distribution of the graph. Scale-free networks were originally defined as networks that show a degree distribution that follows a power law of the form $P(k) \sim k^{-y}$ with an exponent y of 3 (Barabasi and Albert, 1999; Grigorov, 2005). Recent studies have also concluded scale-free properties for networks of exponents $2 < y < 3$ (Goh et al., 2001, 2002; Grigorov, 2005) and real-world biological networks were classified with exponents around 2 (Goh et al., 2001). Most importantly, a scale-free architecture is characterized by a power-law scaled connectivity distribution, in contrast to random networks that show a Poisson shaped connectivity distribution (Barabasi and Bonabeau, 2003).

Computed network characteristics

For each of the individual functional connectivity graphs Gnet the graph characteristics Cnet and Lnet were computed for varying T ranging from 0 to 0.7, with steps of 0.05 (Fig. 1, panel g). For each thresholded Gnet, h random graphs $G_h$random were formed with similar k and $P(k)$ as Gnet (Fig. 1, panel e). Sporns and Zwi (2004) have suggested that statistical comparisons should be performed between networks of similar degree distributions. However, theoretical random networks have a Poisson shaped degree distribution and this might differ from the degree distribution of Gnet. Therefore, for the creation of each random graph $G_h$random, Gnet was used as the original starting point and then for each node i the paths of node i were randomly distributed to random selected nodes in the graph, keeping the total number of connections of node i fixed (Fig. 1, panel e). This procedure was repeated for all nodes in Gnet until the connection topology of the original matrix (i.e. Gnet) was randomized, resulting in a random graph $G_h$random with a degree distribution similar to that of Gnet (Fig. 1, panel f).

For each of the resulting random graphs $G_h$random the graph characteristics $C_h$random and $L_h$random were computed (Fig. 1, panel g). From these h random graphs Gnet, Crandom and Lrandom were computed as:

$$C\text{random} = \frac{1}{h} \sum C_h\,\text{random} \quad (6)$$

$$L\text{random} = \frac{1}{h} \sum L_h\,\text{random}. \quad (7)$$

Next, γ, λ and the small-world index sigma were calculated for varying T (Fig. 1, panel h and i). h was set to 20 for $0.40 \leq T \leq 0.7$, to 10 for $0.2 \leq T < 0.40$ and to 5 for $T < 0.2$ for computational reasons. In total, this resulted in 215 different thresholded graphs (i.e. Gnet and $G_h$random) of size N per individual dataset.

For each individual dataset, the frequency of occurrence of a voxel in Gnet having k connections was computed (Fig. 1, panel j). This resulted in an individual connectivity degree distribution $P(k)$ for each of the varying correlation thresholds T.

In addition, to account for the varying effects of T on the individual connectivity graphs, Cnet, Lnet, Crandom, Lrandom, γ, λ, sigma and $P(k)$ were also computed for a number of fixed k. Keeping T fixed could have varying effects on the connectivity graphs over the group of subjects, as the individual datasets are likely to vary in overall connectivity. Therefore, an additional analysis was performed, in which the average connectivity degree k was kept fixed over the individual datasets. For each fixed k, M was thresholded with a computed T that corresponded exactly to a connectivity degree of k for that particular dataset and Cnet, Lnet, Crandom, Lrandom, γ, λ, sigma and $P(k)$ were computed. k varied for 15 settings, being 4000, 2000, 1500, 1000–100 (with steps of 100), 50 and 20. The number of random graphs h per fixed k for the computation of Crandom and Lrandom was set to 20 for $20 \leq k \leq 700$, to 10 for $700 < k \leq 1000$ and to 5 for $k \geq 1500$ for computational reasons. This resulted in 240 different graphs (including both Gnet and $G_h$random) of size N per individual dataset.

For each individual dataset, this procedure resulted in a set of graph characteristics of the individual connectivity networks *G*net, including the clustering-coefficient *C*net and *C*random, path length *L*net and *L*random, γ, λ and the small-world index sigma (Fig. 1). These resulting graph characteristics were averaged over the group of 28 subjects. In addition, the individual connectivity distributions were averaged over the group of subjects and fitted a power-law distribution

$$P(k) = ck^{-\gamma}, \quad (8)$$

as an indication of a possible scale-free organization of the functionally connected human brain.

Connectivity map

A scale-free network is characterized by the existence of a small number of nodes that have many more connections than the other nodes of the network. The nodes that have such a high connectivity degree are referred to as hub-nodes and are suggested to play an important role in the overall network organization (Barabasi and Albert, 1999; Grigorov, 2005). An exploratory analysis was performed to examine the spatial location of these hub-regions in the brain. A group connectivity map (group *k*map) was computed that reflected the topology of functional connectivity in the brain. First, individual connectivity maps (*k*maps) were formed by flagging all sub-cortical and cortical voxel with their connectivity degree. In this exploratory analysis, the voxel-wise connectivity degrees were calculated for a *T* of 0.4. Second, the individual *k*maps were smoothed with an 8 mm FWHM smoothing kernel (i.e. 2 fMRI voxels) to improve cross-subject overlap. The individual *k*maps were then scaled between 0 and 1, by dividing the connectivity degree values by the maximum value of the individual *k*map to normalize the connectivity values over the group of subjects. Finally, a group *k*map was formed by averaging the scaled individual *k*maps. Voxels that showed a connectivity degree that was much higher than the average degree were marked as potential hub-voxels. An exploratory threshold was defined as the top 2.5% of the voxels that showed the highest connectivity degrees. This threshold was defined by sorting all group-wise connectivity degree values and selecting the first of the top 2.5% highest values. The voxels that showed a connectivity degree above this 2.5% threshold were marked as potential hub-regions.

Results

Clustering-coefficient and path length

The results for the group averaged clustering-coefficient *C*net and *C*random and their dependence on *T* are shown in Fig. 2a. *C*net was found to be significant higher than *C*random, for all values of $T \geq 0.10$ [$p < 0.01$, Bonferroni corrected], indicating a higher level of ordering in the resting-state functional graph in comparison to a random connected graph. *C*random was calculated as the average clustering-coefficient of a set of random graphs ($h = 20$ or $h = 10/5$ for less sparse graphs, see Materials and methods section) with a similar connectivity degree *k* and distribution *P(k)* as *G*net. As expected, *C*net decreased with increasing *T*, as more and more paths in graph *G* are removed. For the computation of *C*net and *C*random disconnected voxels were removed from the graph (see Materials and methods section). The results for the group averaged characteristic path length *L*net and *L*random and their relation to *T* are shown in Fig. 2b. The path length *L*net of the functional

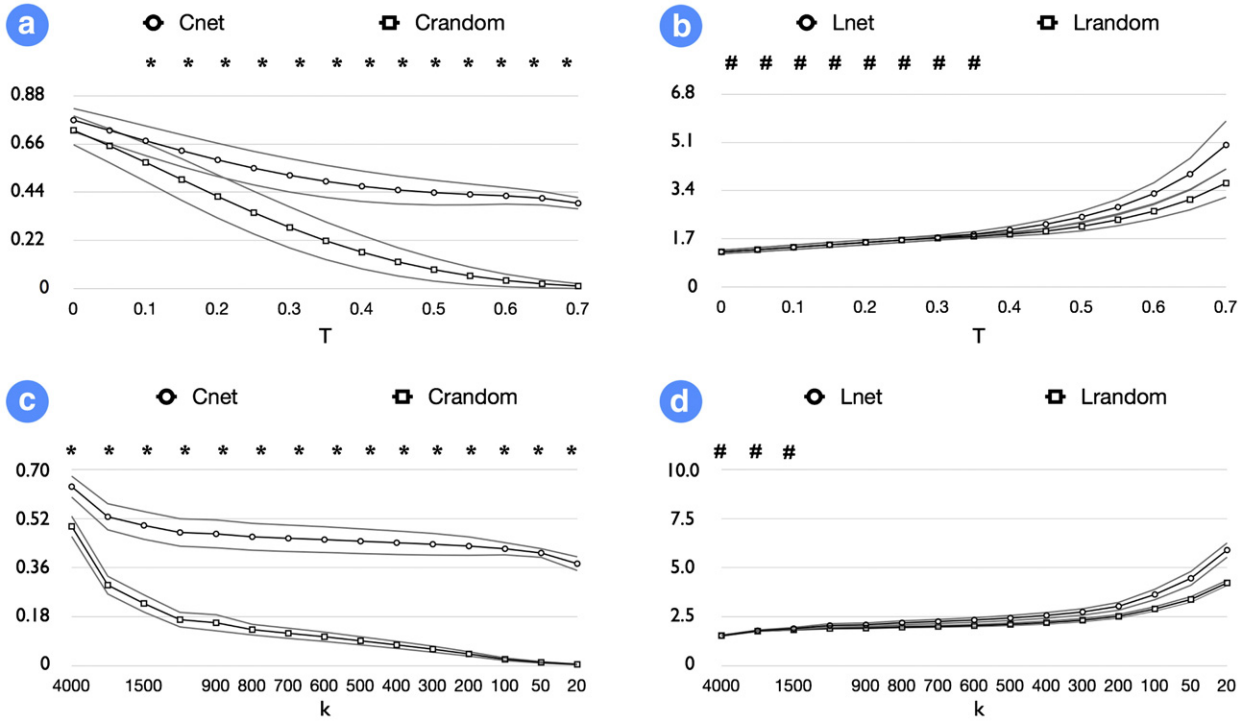

Fig. 2. Group averaged clustering-coefficient and characteristic path length for varying *T* and varying *k*. Panel a shows the group averaged clustering-coefficient *C*net of the graph representation *G*net of the functionally connected brain and its relation to the cut-off threshold *T*, as well as the clustering-coefficient *C*random of a random graph with similar connectivity degree *k* and distribution *P(k)* as *G*net. *C*net was found to be significant higher than *C*random for $T \geq 0.10$ [$p < 0.01$, Bonferroni corrected, indicated by *]. Panel b shows the group averaged characteristic path length *L*net of *G*net as well as the characteristic path length *L*random of a random graph with similar connectivity degree *k* and connectivity distribution *P(k)* and its dependence on *T*. *L*net was found not to be different from *L*random for $T \leq 0.35$ [$p < 0.01$, Bonferroni corrected, indicated by #]. Standard deviations are plotted in grey, expressing a low level of inter-subject variability over the group of subjects. No outliers were present in the group dataset. Panels c and d show *C*net, *C*random and *L*net, *L*random and their relation to the average connectivity degree *k*. *C*net was significant higher than *C*random for $k \leq 4000$ [$p < 0.01$, Bonferroni corrected, indicated by *] and *L*net was found not to be different from *L*random for $k \geq 1500$ [$p < 0.01$, Bonferroni corrected, indicated by #]. Standard deviations of the group averaged clustering-coefficient and path length values are plotted in grey.

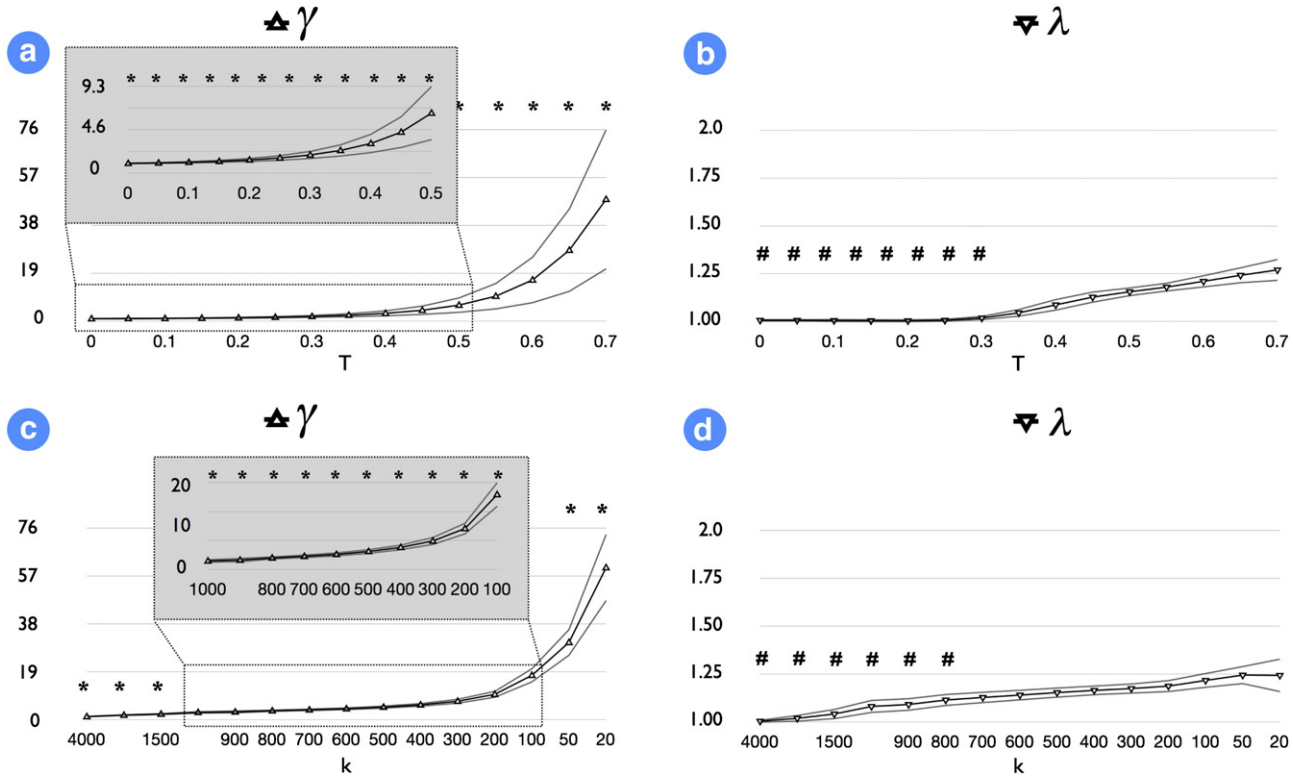

Fig. 3. γ and λ. Panels a and b shows γ, defined as *C*net/*C*random and λ, defined as *L*net/*L*random and their dependence on the threshold *T*. γ was found to be significant >1 for all values of *T* [$p<0.01$, Bonferroni corrected, indicated by *]. λ was found not to be different from 1 for $T<0.4$ [$p<0.01$, Bonferroni corrected, indicated by *]. Panels c and d shows γ and λ and their dependence on *k*. γ was significant >1 for $k\leq4000$ [$p<0.01$, Bonferroni corrected, indicated by *] and λ was found not to be different from 1 for $k\geq800$ [$p<0.01$, Bonferroni corrected, indicated by #]. Error-bars show the standard deviations of the group averaged γ and λ and indicate a low level of inter-subject variability of γ and λ over the group of subjects.

connected graph was found not to be significant different from the average path length of a random network with similar *k* and *P(k)* for $T\leq0.35$ [$p<0.01$, Bonferroni corrected]. As shown in Fig. 2b, *L*net increased with increasing *T*. With increasing *T*, more paths are removed and an increasing number of paths have to be crossed to travel from voxel *i* to voxel *j*, resulting in an overall increasing path length. The results for *C*net, *C*random, *L*net and *L*random and their relation to *k* are given in Figs. 2c and d. *C*net was found to be significant higher than *C*random for $k\leq2000$ [$p<0.01$, Bonferroni corrected]. *L*net and *L*random were found not to be different for $k\geq1500$ [$p<0.01$, Bonferroni corrected]. Error-bars in Fig. 2 show the standard deviations of the group averaged *C*net, *C*random, *L*net, and *L*random. The low standard deviations indicated a low level of inter-subject variability. The group data did not show any outliers.

γ *and* λ

Figs. 3a and b show the group averaged γ and λ over the group of subjects for varying *T*. γ was significantly higher than 1 for all *T* [$p<0.01$, Bonferroni corrected], λ was found not to be different from 1 for $T\leq0.40$ [$p<0.01$, Bonferroni corrected]. Figs. 3c and d show γ and λ and their dependence on *k*. γ was significantly higher than 1 for all *k* [$p<0.01$, Bonferroni corrected] and λ was found not to be different from 1 for $k\geq800$ [$p<0.01$, Bonferroni corrected]. Error-

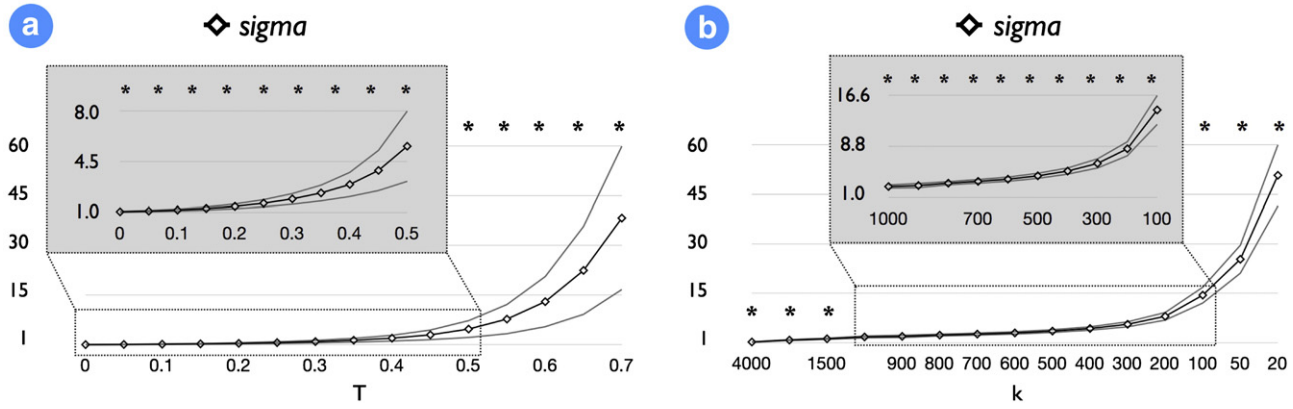

Fig. 4. Small-world index sigma. Panels a and b show the small-world index sigma (i.e. γ/λ) for varying *T* and varying *k*. Sigma was found to be significant >1 for all *T* (a) and for all $k\leq4000$ (b) [$p<0.01$, Bonferroni corrected, indicated by *], suggesting a small-world organization of the functionally connected brain at a voxel scale. Standard deviations over the group of subjects are plotted in grey and suggest a low level of inter-subject variability.

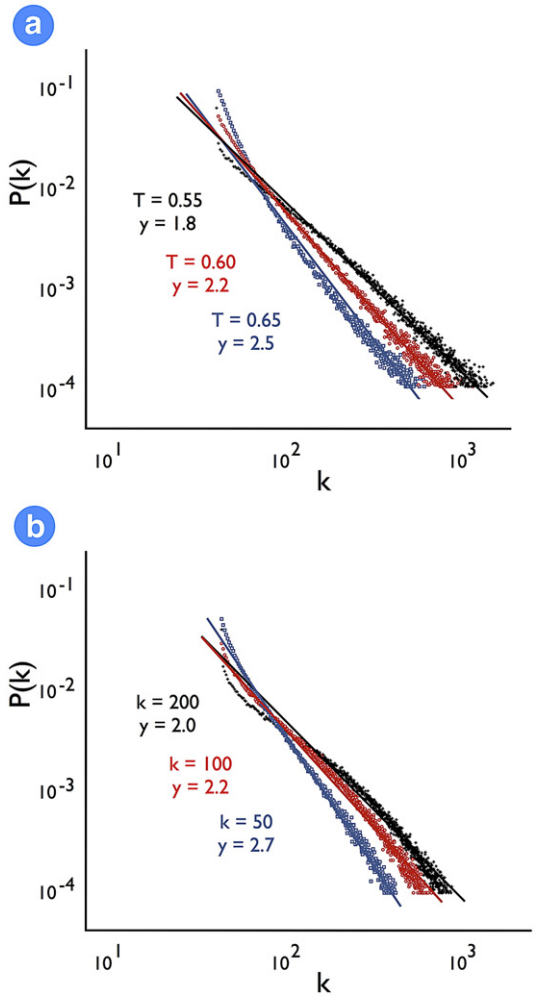

Fig. 5. Connectivity distribution. Panel a shows the connectivity distribution $P(k)$ and fitted power-law functions for T=0.55 (black cross), 0.60 (red circle) and 0.65 (blue square). Panel b shows the connectivity distribution $P(k)$ and the fitted power-law functions for k=200 (black cross), 100 (red circle) and 50 (blue square). The distributions followed a power-law function $P(k) \sim k^{-y}$, with exponents y close to 2, suggesting a possible scale-free organization of the functionally connected human brain at a voxel scale.

bars in Fig. 3 show the standard deviations over the group of subjects, indicating the level of inter-subject variability (no outliers were found).

Small-world index sigma

The group averaged small-world index sigma for T varying between 0 and 0.7 and k varying between 4000 and 20 are given in Figs. 4a and b. Sigma was found to be significant higher than 1 for all $T \geq 0.1$ and for all k, suggesting a small-world organization of Gnet. Standard deviation error-bars in Fig. 4 express the level of inter-subject variability (no outliers were found).

Connectivity distribution

The group averaged connectivity distribution $P(k)$ is shown in Fig. 5a for a threshold T of 0.55, 0.60 and 0.65. The group averaged $P(k)$ suggested to follow a power-law scaling decaying as $P(k) \sim c\, k^{-y}$ with exponents close to 2 (T=0.55, y=1.8; T=0.60, y=2.2; T=0.65, y=2.5). The average connectivity distribution $P(k)$ for fixed k of 200, 100 and 50 are shown in Fig. 5b, together with a fitted power-law distributions with exponents close to 2 (k=200, y=2.0; k=100, y=2.2; k=50, y=2.7). No outliers were found in the group of subjects.

Connectivity map

Fig. 6 depicts the regions that showed the highest (scaled) connectivity degree values of the group $k$map for a T of 0.4. The top 2.5% of the highest connectivity degree values reflected a threshold of 0.61, the maximum found group averaged (scaled) connectivity value was 0.82. Fig. 6 depicts the regions that showed a connectivity degree above this 2.5% threshold, i.e. the voxels that showed the largest number of connections in Gnet. These regions included the right and left thalamus, bilateral superior temporal lobe (BA 22/40/42), bilateral anterior cingulate cortex (BA 24) and bilateral posterior cingulate cortex/(pre)cuneus (BA 30/31/18).

Discussion

The main findings of this study are a possible *small-world* and *scale-free* organization of the functionally connected human brain

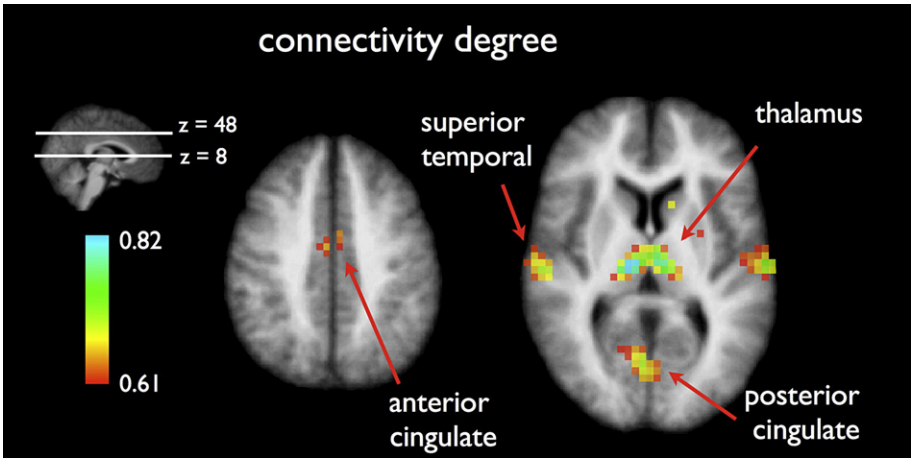

Fig. 6. Potential hub-regions of the functional brain. An additional analysis was performed to examine the topology of functional connectivity in the brain and to look for the location of potential hub-regions. Individual connectivity maps were computed by flagging each voxel with its connectivity degree (i.e. the number of connections) for a T of 0.4. Individual connectivity maps were smoothed (8mm FWHM, note that smoothing may lead to an underestimation of the connectivity degree of thin cortical regions) to improve cross-subject overlap and scaled between 0 and 1 (see for details Materials and method section). Next, a group connectivity map was computed by averaging the scaled individual connectivity maps. An exploratory threshold was set to the top 2.5% of the voxels that showed the highest scaled connectivity degree (i.e. the highest number of functional connections), reflecting a threshold of 0.61. The maximum value of the group connectivity map was found to be 0.82, indicating the maximum found connectivity degree. Figure shows the regions that showed a connectivity degree above the 2.5% threshold, indicating the regions with the highest connectivity degree of the functionally connected brain. These regions included the left and right thalamus, bilateral superior temporal lobe and anterior and posterior cingulate cortex/(pre)cuneus. The high connectivity degree of these voxels marks these regions as potential hub-regions.

on a voxel level. Resting-state fMRI of 28 healthy subjects was acquired on a 3 Tesla MR scanner. For each individual dataset, a network was constructed out of all cortical and sub-cortical voxels with connections between functionally linked voxels. From this connectivity network a number of graph organization characteristics were computed. The clustering-coefficient turned out to be much higher than the clustering-coefficient of a comparable random network, but still with an average short path length (Fig. 2). This graph topology was reflected in a γ of >1 and a λ of ≈1 and a small-world index >1 (Figs. 3 and 4), suggesting a small-world organization (Humphries et al., 2006; Watts and Strogatz, 1998) of the functionally connected brain during a resting-state. Furthermore, the connectivity distribution *P(k)* suggested to follow a power-law distribution for a range of fixed *T* and fixed average connectivity degree *k*. These results suggest a possible scale-free topology of the functionally connected brain (Fig. 5) (Barabasi and Bonabeau, 2003). As far as we know, this is the first study that investigated a small-world and scale-free organization of functional connectivity in the human brain on a voxel scale during a resting-state.

Small-world networks are characterized by a high representation of strongly interconnected sub-networks, a property that follows directly from the high clustering-coefficient (Sporns and Zwi, 2004; Watts and Strogatz, 1998) and this suggests a high resilience to random loss of connections (Kaiser et al., 2007). The overall short characteristic path length demonstrates that nodes of the same sub-network and that of different sub-networks are generally connected by short paths (Watts and Strogatz, 1998), suggesting a high level of global communication efficiency (Latora and Marchiori, 2001). Furthermore, a possible a scale-free topology of the functionally connected brain suggests that the overall short path length is mediated by a small number of highly connected hub-regions. Scale-free networks show a surprising robustness to random failure of nodes, but are known to be vulnerable to target attack on the hubs (Albert et al., 2000; Callaway et al., 2000). A scale-free topology ensures an efficient and robust transport and flow processing in the network by avoiding congestion of information flow (Grigorov, 2005; Toroczkai and Bassler, 2004). The formation of scale-free networks has been suggested to follow a 'preferential attachment' principle, suggesting that new connections prefer to connect to nodes that already have a high number of connections (Albert and Barabasi, 2000). This effect is believed to be the result of a self-organized criticality principle (Levina et al., 2007). Taken together, a combined small-world and scale-free architecture ensures an optimal form of network organization, forming a balance between maximum communication efficiency (Latora and Marchiori, 2001) and minimum wiring (Barabasi and Bonabeau, 2003; Mathias and Gopal, 2001).

These results raise the question about the functional implication of a possible small-world and scale-free organization of the human brain (Sporns et al., 2004). One interpretation of our results is that it might reflect an optimal minimized architecture (Mathias and Gopal, 2001) of the brain in which information is processed by highly interconnected networks of regions and efficiently transferred between networks for further processing (Achard and Bullmore, 2007; Liu et al., 2008; Salvador et al., 2005a). Indeed, recent group resting-state studies have suggested the consistent formation of a number of resting-state networks of regions that show a high level of resting-state functional connectivity (Beckmann et al., 2005; Damoiseaux et al., 2006; Van den Heuvel et al., 2008). Such an architecture of strongly connected networks is coherent with the observed high level of clustering. The overall short path length suggests an efficient communication transfer between regions that form such resting-state networks as well as a streamlined information transfer between regions of different networks. Furthermore, the observed power-law scaling of the connectivity distribution suggests a possible scale-free topology of the functional brain, which might indicate that most voxels are only connected to voxels within a specific sub-network and that inter-network communication is mediated by a small number, but highly connected hub-regions. An exploratory analysis of the spatial topology of functional connectivity in the brain revealed a number of regions that showed a much higher connectivity degree than the rest of the nodes of the brain network (Fig. 6). These regions included the left and right thalamus and cortical regions overlapping the superior temporal lobe and anterior and posterior cingulate cortex and (pre) cuneus. The high connectivity degree marks these regions as potential hub-regions of the functional brain. These regions show large overlap with the hub-regions found by Achard et al. (2006). Future studies are aimed to further investigate the key role of these hub-regions in the overall architecture of the functionally connected brain. Taken together, we believe that our results suggest a highly efficient organization of the functional brain, with an optimal balance between local and global connectivity (Watts and Strogatz, 1998), maximum communication efficiency (Achard and Bullmore, 2007; Latora and Marchiori, 2001) and minimum functional wiring between the regions of the brain (Mathias and Gopal, 2001).

In this study, a voxel-wise approach was used to investigate the organization of functional connectivity. Our results are coherent with the results of a number of recent studies reporting on a small-world organization of inter-regional functional connectivity in the human brain (Achard and Bullmore, 2007; Achard et al., 2006; Liu et al., 2006, 2008; Salvador et al., 2005a; Sporns and Zwi, 2004). These studies have mainly focused on the organization of functional connectivity between brain regions, by using a predefined parcellation of the brain in around 90 regions. However, using a predefined regional template limits the examination to inter-regional connectivity and requires a model-based definition of such regions. In this study, both inter-regional as well as intra-regional connectivity was considered, forming a network out of voxels rather than 90 large regions. Using a voxel-based method, our results support previous regional-based findings and contribute to the idea of a small-world architecture of the human brain (Achard et al., 2006; Eguiluz et al., 2005; He et al., 2007; Liu et al., 2006, 2008; Salvador et al., 2005a; Sporns and Zwi, 2004). In addition, our results suggest a possible scale-free organization of the functional brain network. The results from two previous studies investigating such a scale-free topology of the brain have been inconclusive. A recent study of Achard et al. (2006) investigating inter-regional resting-state functional connectivity reported a small-world, but not a scale-free organization of the human brain. In contrast, a study of Eguiluz et al. (2005) showed a combined small-world and scale-free topology. However, the results of that study were based on voxel-based task-induced fMRI measurements, rather than resting-state recordings. Task-induced fMRI recordings could have had an effect on the overall temporal activation patterns of the brain and as a result on the topology of functional connectivity. Therefore, in our study correlations between resting-state time-series were used as a more general measure of functional connectivity (Achard et al., 2006; Greicius et al., 2003; Salvador et al., 2005b). The observed power-law scaling of the connectivity distribution in our study suggests a possible scale-free organization of the functionally connected brain. One explanation of the differentiating results of our study and the study of Achard et al. (2006), concerning a possible scale-free organization, might lie in the included intra-regional connectivity in this study. Achard et al. focused on the organization of inter-regional functional connectivity between 90 brain regions, whereas in our study resting-state functional connectivity was investigated on a voxel scale, including both inter-regional as well as intra-regional connectivity. Interestingly, this differentiation in network topology of the brain might suggest a different organization of inter-regional connectivity and connectivity between smaller regions (i.e. voxels). One possible interpretation of our results might be that large brain regions are on average connected with around the same number of other brain regions, while sub-regions have on average a low number of connections, but still stay globally connected through means of a small number of highly connected hub-regions.

The functional brain was represented as a network of small brain regions (i.e. voxels), without incorporating any information about the structural connections of the brain. An increasing body of evidence suggests a direct relation between these two forms of connectivity. For example, anatomical networks have been reported to show a similar small-world organization (Hagmann et al., 2007; He et al., 2007). In addition, networks of brain regions showing complex functional dynamics have been suggested to share common structural organization characteristics (Sporns et al., 2002, 2000). Furthermore, regions of widespread functionally connected resting-state networks have been found to be connected by cortico-cortical anatomical tracts (Greicius et al., in press; Lowe et al., 2008). Taken together, these results suggest a direct link between the functional and structural organization of the brain and a combined analysis could provide valuable information about the general architecture of the brain (Honey et al., 2007; Sporns et al., 2004, 2000).

In this study we mainly focused on the overall connectivity architecture of the functionally connected human brain. However, the used voxel-wise approach allows for a much more specific examination of the functional brain network. It allows for the examination of functional connections on a high spatial resolution, for example the identification of inter-hemispheric and intra-hemispheric connections and a classification of their role in the network. Future studies are aimed to examine the specific role of different functional connections in the overall architecture of the brain network.

Analyzing the small-world properties of the functionally connected brain can be of importance in future clinical studies. Recent studies have suggested a disrupted small-world functional connectivity organization in schizophrenia in multiple EEG frequency bands (Micheloyannis et al., 2006; Rubinov et al., in press). Furthermore, a recent resting-state fMRI study has reported disrupted small-world networks in schizophrenia (Liu et al., 2008). The use of a voxel-wise resting-state fMRI method could contribute to this field. It allows for the examination of disrupted functional connectivity in patients in high detail, providing information on which regions are affected. In general, examining the architecture of the brain on a voxel scale could provide a more detailed insight in the suggested disrupted functional organization in brain diseases, like schizophrenia (Liu et al., 2008) and Alzheimer's disease (Stam et al., 2007).

Some limitations to this study have to be considered in interpreting its results. First, the exact neuronal correlate of resting-state functional connectivity is not fully understood. Although, it is believed that the coherency between the rest-recorded BOLD-sensitive fMRI time-series is related to a coherency in the underlying neuronal activation patterns of these regions (Biswal et al., 1997; Buckner and Vincent, 2007; Cordes et al., 2001; Greicius et al., 2003; Salvador et al., 2005a), it has also been suggested that physiological temporal patterns like respiratory and cardiac oscillations could confound the BOLD signal (Cordes et al., 2001; Wise et al., 2004). In this study, a high fMRI temporal acquisition was used to minimize the possible backfolding of cardiac and respiratory patterns into the lower frequencies of interest, enabling the proper filtering of these high frequency temporal patterns (Cordes et al., 2001, 2000). However, cardiac related frequencies of >1 Hz could still be aliased into the lower frequencies of interest. In addition, there has been suggested that other non-neuronal related low frequency oscillations, like possible variations in heart rate or interactions between cardiac and respiratory signals can be present in the low resting-state frequencies of interest (~0.01–0.1 Hz), making the resting-state correlations less specific (Birn et al., 2008). Second, it should be noted that fMRI images show a certain level of intrinsic spatial smoothness and this could introduce artificial inter-voxel correlations that are not related to neuronal activity. Data interpolation as a result of the normalization of the fMRI time-series may further enhance this effect. Spatial smoothness could lead to an overestimation of the local inter-voxel correlations in *G*net and introduce a bias in the computation of the graph characteristics and have an effect on the scale-free aspects of the data. In this study, *G*random was formed by randomizing all connections of *G*net to maintain a similar connectivity distribution (Sporns and Zwi, 2004). However, when forming a comparable random graph *G*random, potential intrinsic spatial smoothness present in the fMRI recordings (and therefore present in *G*net) is destroyed. To examine the effect of spatial smoothness on the graph characteristics a post-hoc analysis was performed, in which the formation of *G*random was adjusted by redistributing only those connections of *G*net that connected voxels that were spatially separated by more than 10 mm (>2.5 voxels) (28 subjects, *T* varying between 0 and 0.7 with steps of 0.1, the number of random graphs *h* set to 1). As such, *G*random was formed in a much more conservative manner, maintaining *all* local connections that were present in *G*net, and thus ensuring a similar intrinsic smoothness profile as *G*net. Constructing *G*random in this alternative way did not change the nature of our results. As expected, the only difference found was that *C*random was slightly higher than the original *C*random (and only for high *T*). This difference was likely to result from the fact that *G*random was now more similar to *G*net. Taken together, these additional results suggest that the intrinsic smoothness of fMRI data has only a minor influence on the computation of the graph characteristics and does not affect the main results of this study. In addition, to test the influence of the normalization step on the final results, a second post-hoc analysis was performed, in which *G*net was based on the native (non-normalized) individual time-series, rather than the normalized fMRI time-series. Analyzing the data in native space (i.e. non-normalized) did not change the nature of the results, which suggests that the normalization step had only a minor influence on the computation of the graph characteristics. Third, as in all resting-state fMRI studies using graph analysis, partial voluming effects (due to the relatively large fMRI voxels of 3 to 4 mm) and the inclusion of misclassified CSF or white matter voxels into *G*net could potentially introduce artificial correlations that are not related to neuronal synchronization. As a result, they could (in theory) explain the found effects. To examine the effects of white matter and CSF voxels on the computed graph statistics an additional post-hoc analysis was performed, in which the connectivity graphs were formed out of all classified white matter (*G*wm) and CSF (*G*csf) voxels. From these connectivity graphs the general graph characteristics were computed, in a similar way as described in the main analysis (Fig. 1). Both *G*wm and *G*csf showed a high clustering-coefficient and a much higher path length than *G*net, typical for networks with a so-called 'regular' organization, lacking the existence of long distance connections critical for a *small-world* organization. In addition, the degree distribution of *G*wm and *G*csf did not show the typical scale-free organization as found for *G*net. This post-hoc analysis suggests that white matter and CSF related correlations show a different organization in comparison to correlations between grey matter voxels and that they are likely to only minimally influence the computed graph characteristics of *G*net. Fourth, as with all cross-correlation methods, the association between points is based on linear effects. Other measures like s*ynchronization likelihood* have been successfully introduced as a measure of nonlinear coupling of EEG and MEG signals (Stam et al., 2003) and could make a valuable contribution to resting-state fMRI investigations. In addition, methods to calculate the network characteristics of weighted graphs have been suggested, as well as measures of global and local communication efficiency (Achard and Bullmore, 2007; Latora and Marchiori, 2001; Reijneveld et al., 2007; Stam and Reijneveld, 2007) and used as an effective method to control for disconnected nodes that are likely to arise with increasing cut-off thresholds (Ponten et al., 2007). In this study, the traditional definition of the clustering-coefficient was used (Achard and Bullmore, 2007; Stam and Reijneveld, 2007; Watts and Strogatz, 1998), but more advanced versions have been suggested. Soffer and Vazquez (2005) showed that the traditional definition is biased to the number of connections of a node and suggested a non-biased

definition. Future studies are aimed to investigate the use of these novel measures of network dynamics in a voxel-based approach.

In this study, the organization of functional connectivity in the human brain was examined on a voxel scale. Graph theory was used to investigate 3 T resting-state fMRI recordings of 28 healthy subjects by forming individual networks out of all cortical and sub-cortical voxels, with connections between functionally connected voxels. The use of a voxel-wise approach allowed for the examination of inter-regional connectivity as well as intra-regional connectivity. Our results suggest a possible combined *small-world* and *scale-free* organization of the functionally connected human brain.

Appendix A. Supplementary data

Supplementary data associated with this article can be found, in the online version, at doi:10.1016/j.neuroimage.2008.08.010.

References

Achard, S., Bullmore, E., 2007. Efficiency and cost of economical brain functional networks. PLoS. Comput. Biol. 3, e17.

Achard, S., Salvador, R., Whitcher, B., Suckling, J., Bullmore, E., 2006. A resilient, low-frequency, small-world human brain functional network with highly connected association cortical hubs. J. Neurosci. 26, 63–72.

Aertsen, A.M., Gerstein, G.L., Habib, M.K., Palm, G., 1989. Dynamics of neuronal firing correlation: modulation of "effective connectivity". J. Neurophysiol. 61, 900–917.

Albert, R., Barabasi, A.L., 2000. Topology of evolving networks: local events and universality. Phys. Rev. Lett. 85, 5234–5237.

Albert, R., Jeong, H., Barabasi, A.L., 2000. Error and attack tolerance of complex networks. Nature 406, 378–382.

Barabasi, A.L., Albert, R., 1999. Emergence of scaling in random networks. Science 286, 509–512.

Barabasi, A.L., Bonabeau, E., 2003. Scale-free networks. Sci. Am. 288, 60–69.

Beckmann, C.F., DeLuca, M., Devlin, J.T., Smith, S.M., 2005. Investigations into resting-state connectivity using independent component analysis. Philos. Trans. R. Soc. Lond. B. Biol. Sci. 360, 1001–1013.

Birn, R.M., Diamond, J.B., Smith, M.A., Bandettini, P.A., 2006. Separating respiratory-variation-related fluctuations from neuronal-activity-related fluctuations in fMRI. Neuroimage 31, 1536–1548.

Birn, R.M., Smith, M.A., Jones, T.B., Bandettini, P.A., 2008. The respiration response function: the temporal dynamics of fMRI signal fluctuations related to changes in respiration. Neuroimage 40, 644–654.

Biswal, B., Yetkin, F.Z., Haughton, V.M., Hyde, J.S., 1995. Functional connectivity in the motor cortex of resting human brain using echo-planar MRI. Magn. Reson. Med. 34, 537–541.

Biswal, B.B., Van Kylen, J., Hyde, J.S., 1997. Simultaneous assessment of flow and BOLD signals in resting-state functional connectivity maps. NMR. Biomed. 10, 165–170.

Breakspear, M., Terry, J.R., Friston, K.J., Harris, A.W., Williams, L.M., Brown, K., Brennan, J., Gordon, E., 2003. A disturbance of nonlinear interdependence in scalp EEG of subjects with first episode schizophrenia. Neuroimage 20, 466–478.

Buckner, R.L., Vincent, J.L., 2007. Unrest at rest: default activity and spontaneous network correlations. Neuroimage 37, 1091–1096.

Buzsaki, G., Draguhn, A., 2004. Neuronal oscillations in cortical networks. Science 304, 1926–1929.

Callaway, D.S., Newman, M.E., Strogatz, S.H., Watts, D.J., 2000. Network robustness and fragility: percolation on random graphs. Phys. Rev. Lett. 85, 5468–5471.

Collins, D.L., Neelin, P., Peters, T.M., Evans, A.C., 1994. Automatic 3D intersubject registration of MR volumetric data in standardized Talairach space. J. Comput. Assist. Tomogr. 18, 192–205.

Cordes, D., Haughton, V.M., Arfanakis, K., Wendt, G.J., Turski, P.A., Moritz, C.H., Quigley, M.A., Meyerand, M.E., 2000. Mapping functionally related regions of brain with functional connectivity MR imaging. AJNR. Am. J. Neuroradiol. 21, 1636–1644.

Cordes, D., Haughton, V.M., Arfanakis, K., Carew, J.D., Turski, P.A., Moritz, C.H., Quigley, M.A., Meyerand, M.E., 2001. Frequencies contributing to functional connectivity in the cerebral cortex in "resting-state" data. AJNR. Am. J. Neuroradiol. 22, 1326–1333.

Damoiseaux, J.S., Rombouts, S.A., Barkhof, F., Scheltens, P., Stam, C.J., Smith, S.M., Beckmann, C.F., 2006. Consistent resting-state networks across healthy subjects. Proc. Natl. Acad. Sci. U. S. A. 103, 13848–13853.

Eguiluz, V.M., Chialvo, D.R., Cecchi, G.A., Baliki, M., Apkarian, A.V., 2005. Scale-free brain functional networks. Phys. Rev. Lett. 94, 018102.

Fox, M.D., Raichle, M.E., 2007. Spontaneous fluctuations in brain activity observed with functional magnetic resonance imaging. Nat. Rev. Neurosci. 8, 700–711.

Fox, M.D., Snyder, A.Z., Vincent, J.L., Corbetta, M., Van Essen, D.C., Raichle, M.E., 2005. The human brain is intrinsically organized into dynamic, anticorrelated functional networks. Proc. Natl. Acad. Sci. U. S. A. 102, 9673–9678.

Friston, K.J., Frith, C.D., Liddle, P.F., Frackowiak, R.S., 1993. Functional connectivity: the principal-component analysis of large (PET) data sets. J. Cereb. Blood Flow Metab. 13, 5–14.

Goh, K.I., Kahng, B., Kim, D., 2001. Universal behavior of load distribution in scale-free networks. Phys. Rev. Lett. 87, 278701.

Goh, K.I., Oh, E., Jeong, H., Kahng, B., Kim, D., 2002. Classification of scale-free networks. Proc. Natl. Acad. Sci. U. S. A. 99, 12583–12588.

Golay, X., Pruessmann, K.P., Weiger, M., Crelier, G.R., Folkers, P.J., Kollias, S.S., Boesiger, P., 2000. PRESTO-SENSE: an ultrafast whole-brain fMRI technique. Magn. Reson. Med. 43, 779–786.

Greicius, M.D., Krasnow, B., Reiss, A.L., Menon, V., 2003. Functional connectivity in the resting brain: a network analysis of the default mode hypothesis. Proc. Natl. Acad. Sci. U. S. A. 100, 253–258.

Greicius, M.D., Supekar, K., Menon, V., Dougherty, R.F., in press. Resting-state functional connectivity reflects structural connectivity in the default mode network. Cereb. Cortex. (Electronic publication ahead of print).

Grigorov, M.G., 2005. Global properties of biological networks. Drug Discov. Today 10, 365–372.

Gusnard, D.A., Raichle, M.E., Raichle, M.E., 2001. Searching for a baseline: functional imaging and the resting human brain. Nat. Rev. Neurosci. 2, 685–694.

Hagmann, P., Kurant, M., Gigandet, X., Thiran, P., Wedeen, V.J., Meuli, R., Thiran, J.P., 2007. Mapping human whole-brain structural networks with diffusion MRI. PLoS ONE 2, e597.

He, Y., Chen, Z.J., Evans, A.C., 2007. Small-world anatomical networks in the human brain revealed by cortical thickness from MRI. Cereb. Cortex 17, 2407–2419.

Honey, C.J., Kotter, R., Breakspear, M., Sporns, O., 2007. Network structure of cerebral cortex shapes functional connectivity on multiple time scales. Proc. Natl. Acad. Sci. U. S. A. 104, 10240–10245.

Horwitz, B., Warner, B., Fitzer, J., Tagamets, M.A., Husain, F.T., Long, T.W., 2005. Investigating the neural basis for functional and effective connectivity. Application to fMRI. Philos. Trans. R. Soc. Lond. B. Biol. Sci. 360, 1093–1108.

Humphries, M.D., Gurney, K., Prescott, T.J., 2006. The brainstem reticular formation is a small-world, not scale-free, network. Proc. Biol. Sci. 273, 503–511.

Kaiser, M., Martin, R., Andras, P., Young, M.P., 2007. Simulation of robustness against lesions of cortical networks. Eur. J. Neurosci. 25, 3185–3192.

Kiviniemi, V., Kantola, J.H., Jauhiainen, J., Hyvarinen, A., Tervonen, O., 2003. Independent component analysis of nondeterministic fMRI signal sources. Neuroimage 19, 253–260.

Latora, V., Marchiori, M., 2001. Efficient behavior of small-world networks. Phys. Rev. Lett. 87, 198701.

Levina, A., Herrmann, J.M., Geisel, T., 2007. Dynamical synapses causing self-organized criticality in neural networks. Nature Physics 3, 3.

Liu, H., Liu, Z., Liang, M., Hao, Y., Tan, L., Kuang, F., Yi, Y., Xu, L., Jiang, T., 2006. Decreased regional homogeneity in schizophrenia: a resting state functional magnetic resonance imaging study. Neuroreport 17, 19–22.

Liu, Y., Liang, M., Zhou, Y., He, Y., Hao, Y., Song, M., Yu, C., Liu, H., Liu, Z., Jiang, T., 2008. Disrupted small-world networks in schizophrenia. Brain 131, 945.

Lowe, M.J., Dzemidzic, M., Lurito, J.T., Mathews, V.P., Phillips, M.D., 2000. Correlations in low-frequency BOLD fluctuations reflect cortico-cortical connections. Neuroimage 12, 582–587.

Lowe, M.J., Beall, E.B., Sakaie, K.E., Koenig, K.A., Stone, L., Marrie, R.A., Phillips, M.D., 2008. Resting state sensorimotor functional connectivity in multiple sclerosis inversely correlates with transcallosal motor pathway transverse diffusivity. Hum. Brain Mapp. 29 (7), 818–827.

Mathias, N., Gopal, V., 2001. Small worlds: how and why. Phys. Rev. E. Stat. Nonlin. Soft Matter Phys. 63, 021117.

Micheloyannis, S., Pachou, E., Stam, C.J., Breakspear, M., Bitsios, P., Vourkas, M., Erimaki, S., Zervakis, M., 2006. Small-world networks and disturbed functional connectivity in schizophrenia. Schizophr. Res. 87, 60–66.

Neggers, S.F., Hermans, E.J., Ramsey, N.F., 2008. Enhanced sensitivity with fast three-dimensional blood-oxygen-level-dependent functional MRI: comparison of SENSE-PRESTO and 2D-EPI at 3 T. NMR Biomed. 21 (7), 663–676.

Ponten, S.C., Bartolomei, F., Stam, C.J., 2007. Small-world networks and epilepsy: graph theoretical analysis of intracerebrally recorded mesial temporal lobe seizures. Clin. Neurophysiol. 118, 918–927.

Ramsey, N.F., van den Brink, J.S., van Muiswinkel, A.M., Folkers, P.J., Moonen, C.T., Jansma, J.M., Kahn, R.S., 1998. Phase navigator correction in 3D fMRI improves detection of brain activation: quantitative assessment with a graded motor activation procedure. Neuroimage 8, 240–248.

Reijneveld, J.C., Ponten, S.C., Berendse, H.W., Stam, C.J., 2007. The application of graph theoretical analysis to complex networks in the brain. Clin. Neurophysiol. 118, 2317–2331.

Rubinov, M., Knock, S.A., Stam, C.J., Micheloyannis, S., Harris, A.W., Williams, .L.M., Breakspear, M., in press. Small-world properties of nonlinear brain activity in schizophrenia. Hum. Brain Mapp. (Electronic publication ahead of print).

Salvador, R., Suckling, J., Coleman, M.R., Pickard, J.D., Menon, D., Bullmore, E., 2005a. Neurophysiological architecture of functional magnetic resonance images of human brain. Cereb. Cortex 15, 1332–1342.

Salvador, R., Suckling, J., Schwarzbauer, C., Bullmore, E., 2005b. Undirected graphs of frequency-dependent functional connectivity in whole brain networks. Philos. Trans. R. Soc. Lond. B. Biol. Sci. 360, 937–946.

Shmuel, A., Leopold, D.A., 2008. Neuronal correlates of spontaneous fluctuations in fMRI signals in monkey visual cortex: implications for functional connectivity at rest. Hum. Brain Mapp. 29 (7), 751–761.

Soffer, S.N., Vazquez, A., 2005. Network clustering coefficient without degree-correlation biases. Phys. Rev. E. Stat. Nonlin. Soft Matter Phys. 71, 057101.

Sporns, O., 2006. Small-world connectivity, motif composition, and complexity of fractal neuronal connections. Biosystems 85, 55–64.

Sporns, O., Zwi, J.D., 2004. The small world of the cerebral cortex. Neuroinformatics 2, 145–162.

Sporns, O., Tononi, G., Edelman, G.M., 2000. Connectivity and complexity: the relationship between neuroanatomy and brain dynamics. Neural Netw. 13, 909–922.
Sporns, O., Tononi, G., Edelman, G.M., 2002. Theoretical neuroanatomy and the connectivity of the cerebral cortex. Behav. Brain Res. 135, 69–74.
Sporns, O., Chialvo, D.R., Kaiser, M., Hilgetag, C.C., 2004. Organization, development and function of complex brain networks. Trends Cogn. Sci. 8, 418–425.
Stam, C.J., 2004. Functional connectivity patterns of human magnetoencephalographic recordings: a 'small-world' network? Neurosci. Lett. 355, 25–28.
Stam, C.J., Reijneveld, J.C., 2007. Graph theoretical analysis of complex networks in the brain. Nonlinear Biomed. Phys. 1, 3.
Stam, C.J., Breakspear, M., van Cappellen van Walsum, A.M., van Dijk, B.W., 2003. Nonlinear synchronization in EEG and whole-head MEG recordings of healthy subjects. Hum. Brain Mapp. 19, 63–78.
Stam, C.J., Jones, B.F., Nolte, G., Breakspear, M., Scheltens, P., 2007. Small-world networks and functional connectivity in Alzheimer's disease. Cereb. Cortex 17, 92–99.
Sun, F.T., Miller, L.M., D'Esposito, M., 2004. Measuring interregional functional connectivity using coherence and partial coherence analyses of fMRI data. Neuroimage 21, 647–658.
Thirion, B., Dodel, S., Poline, J.B., 2006. Detection of signal synchronizations in resting-state fMRI datasets. Neuroimage 29, 321–327.
Toroczkai, Z., Bassler, K.E., 2004. Network dynamics: jamming is limited in scale-free systems. Nature 428, 716.
Van den Heuvel, M.P., Mandl, R.C., Hulshoff Pol, H.E., 2008. Normalized group clustering of resting-state fMRI data. PLoS ONE 3, e2001.
Watts, D.J., Strogatz, S.H., 1998. Collective dynamics of 'small-world' networks. Nature 393, 440–442.
Wise, R.G., Ide, K., Poulin, M.J., Tracey, I., 2004. Resting fluctuations in arterial carbon dioxide induce significant low frequency variations in BOLD signal. Neuroimage 21, 1652–1664.
Xiong, J., Parsons, L.M., Gao, J.H., Fox, P.T., 1999. Interregional connectivity to primary motor cortex revealed using MRI resting state images. Hum. Brain Mapp. 8, 151–156.